Dynamics of domain walls for split and runaway potentials

Z. Lalak,[1] S. Lola,[2] and P. Magnowski[1]

[1]*Physics Department, University of Warsow, Poland*
[2]*Department of Physics, University of Patras, Greece*

We demonstrate that the evolution of wall-like inhomogeneities in runaway potentials, characteristic of dynamical supersymmetry breaking and moduli stabilization, is very similar to the evolution of domain-wall networks associated with double-well potentials. Instabilities that would lead to a rapid decay of domain walls can be significantly ameliorated by compensation effects between a nondegeneracy of the vacua and a biased initial distribution, which can be naturally expected in a wide class or particle physics models that lead to out-of-equilibrium phase transitions. Within this framework, it is possible to obtain domain walls that live long enough to be relevant for the cosmic power spectrum and galaxy clustering, while being compatible with the observed cosmic microwave background anisotropies.

PACS numbers: 11.27.+d, 98.80.−k

I. INTRODUCTION

The well-known measurements of the anisotropies of the cosmic microwave background radiation (CMBR) by the Wilkinson Microwave Anisotropy Probe (WMAP) [1], in combination with the supernovae type Ia observations [2], imply that the evolution of the Universe is dominated by dark energy and a state parameter that is strongly constrained. Among the most popular scenarios to explain the data is to assume the existence of an inflationary universe with a very small cosmological constant Λ. In principle, possible contributions to dark energy can also be provided from topological defects which are produced at phase transitions in the Universe [3]. An interesting possibility, for instance, would have been that such contributions are provided by domain walls [4] associated with the breaking of discrete symmetries (which arise commonly in a wide class of particle physics models).

Yet another possibility is that there is no discrete symmetry at all. Even then, there could be nearby minima separated by a potential barrier, with initial conditions that result in both minima getting populated with nonzero probabilities. In this case we do not have an exact domain-wall configuration, but (as will become more obvious later) it still makes sense to talk about approximate domain walls that interpolate, in a broader sense, between basins of attraction of nearby local minima. And, in fact, we will show that the dynamics and evolution of the network of inhomogeneities is very similar in both situations—with exact and approximate domain walls. As a specific example of the behavior of the second type we take runaway potentials which appear in models of dynamical supersymmetry breaking, and play an important role in modern attempts at nonperturbative supersymmetry breaking and moduli stabilization. In fact, it has been pointed out by Dine [5], that spatially inhomogeneous field configurations may evolve differently in the expanding Robertson-Walker background than the homogeneous mode. The inhomoge-

neities may help to stabilize the moduli (such as the dilaton or radion) at shallow but finite minima, thus avoiding the Steinhardt-Brustein [6] and Buchmüller [7] effects. At the same time, the energy density inhomogeneities of such configurations may contribute to the shape of the power spectrum of CMBR. In the case of TeV scale supersymmetry breaking this contribution would be unobservable, but the issue of finding the right vacuum remains a valid question independently of the mass scale associated with a runaway potential.

II. COSMOLOGICAL PROBLEMS WITH WALL NETWORKS AND THEIR POSSIBLE RESOLUTION

There are three main problems in cosmological scenarios that involve a significant abundance of domain walls:

(i) Domain walls that could potentially contribute to dark energy, generally predict an equation of state with $-2/3 < w_X < -1/3$, which would be ruled out from the commonly quoted upper bound $w_X < -0.78$ at 95% C.L.

(ii) Domain walls that could enhance the cold dark matter spectrum are in general associated with unacceptably large fluctuations of the CMBR, for the range of parameters that would have been relevant for the formation of structure. For a horizon-size bubble at a redshift z_a, with surface energy σ, the generated anisotropies are given by

$$\delta T/T \sim G_N \sigma R_H(z_a). \qquad (1)$$

(iii) Domain walls in the simplest class of models that evade problem (ii), do not stay around sufficiently, in order to produce density fluctuations that can sufficiently grow to the observed structures [8–10].

The first problem has in fact been addressed in a very convincing way in [11], where the assumptions made in the

choice of priors of the data analysis have been questioned. In fact, it has been shown that, for lower values of the Hubble parameter ($h < 0.65$, as indicated by Sunyaev-Zeldovich and time delays for gravitational lensing observations), and for higher values of the matter density ($\Omega_m > 0.35$, in agreement with measurements of the temperature-luminosity relation of distant clusters observed with the XMM-Newton satellite), domain walls in an inflationary universe can provide a good fit to the WMAP data.

In previous papers [12,13], we have proposed and tested two main frameworks that may naturally arise in standard model extensions for which domain walls can lead to the formation of structure, enhancing the standard cold dark matter spectrum in an inflationary universe, while still be compatible with CMBR. These are the following:

(a) Schemes where the walls are unstable, due to a nondegeneracy of the minima of the potential (as appears naturally in a wide class of superstring models [12]). For a large range of possible parameters, the walls are expected to annihilate before recombination. In this way, although structure can be generated and subsequently grow in consistency with the observations, no unacceptable distortions to the cosmic microwave background radiation are produced.

(b) A second possibility is that, if one of the minima of the potential of the scalar field is favored, then a biased phase transition occurs. As a first step, we showed why such a bias may be expected in post-inflationary, out-of-equilibrium phase transitions [13]. The idea is that, if the interactions of a field are *very weak*, this will not be confined at the top of its potential, but will in fact be centered around a classical value that will be closer to one of the minima of the potential. Quantum fluctuations will move it, but, nevertheless, the bias (offset) will remain. Then, percolation theory indicates that there is a range of natural initial conditions for which walls of finite size (and not of horizon size) are produced inside a sea of the dominant vacuum. While not very accurate, percolation theory allowed us to formulate a qualitative picture of the spatial distribution of the wall-driven overdensities in a postinflationary universe, and to account for the whole range of large scale structure observations. In addition, by studying wall-driven fluctuations at small scales, it has been possible to reproduce the observed distribution of quasars [14].

Subsequently, elaborate numerical simulations seemed to indicate that despite the biasing of the minima, the walls either disappear too fast or stay around for too long [10], implying that they have to be very soft if they are not to lead to unacceptable distortions of the microwave background radiation. In this work, we will give specific examples where this need not be the case, first in biased double-well potentials with nondegenerate minima and second, for the runaway potentials that can be expected in a wide class of supersymmetry breaking models, based on gaugino condensates. This complements the literature on the subject and raises additional possibilities to those that have been considered in the recent years [15–18].

III. BASIC FRAMEWORK FOR OUT-OF-EQUILIBRIUM, BIASED PHASE TRANSITIONS

An elaborate numerical study of the dynamics of domain-wall networks in the case of a scalar field whose potential has two degenerate minima that occur with the same probability, has been provided by Press, Ryden and Spergel [8]; they showed that such networks would rapidly evolve into long domain walls stretching across the Universe whose surface area, and, hence, energy density, persisted for a long time. This resulted to a rapid domination of the energy density of the Universe by these walls and to unacceptably large distortion in the CMBR. Such an initial distribution on a lattice can be described statistically using percolation theory. On a three-dimensional square lattice, there is a critical probability $p_c = 0.311$, above which the associated vacuum will percolate across the entire lattice [19]. It is easy to see that, by initializing both vacua with a probability $p = 1/2$, both vacua propagate across the lattice. Since domain walls lie on the interface between the two different vacua, this implies the formation of domain walls which extend across the entire Universe. This gives a clear mathematical explanation for the Press, Ryden and Spergel result. However, if for one vacuum $p < p_c$, then this vacuum would form finite clusters in the percolating sea of the other one. The domain walls would then be small, finite bags which would disappear relatively rapidly. Similar effects would hold in the case of potentials with nondegenerate minima [12]. Here, the true minimum will be at some stage energetically favored, and domain walls will disappear.

If a phase transition is triggered by fluctuations in a system in thermal equilibrium, and the vacua are truly degenerate, one expects the population probabilities of each vacuum to be equal. However, nonequilibrium phase transitions, which can occur in realistic models of the early Universe, generically lead to a biased choice of vacuum state. Indeed, an out-of-equilibrium scalar field ϕ living on an inflating de Sitter space, observed over a physical volume ℓ^3, breaks into a classical and a quantum piece

$$\phi = \phi_c + \phi_q, \tag{2}$$

where ϕ_c satisfies the classical equation of motion and ϕ_q represents de Sitter space quantum fluctuations. This is illustrated in Fig. 1.

During inflation, and long afterwards, the Hubble term is very large compared to the curvature of the potential and, thus, to a very good approximation, $\phi_c = \vartheta$, where ϑ is an arbitrary constant (to next order, there is a tiny damped
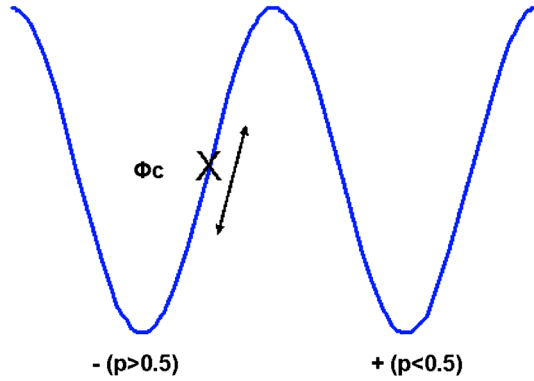
FIG. 1 (color online). Schematic illustration of biased, out-of-equilibrium phase transitions. The initial mean value of the field is shifted towards one of the minima, which occurs with a higher probability.

velocity $\dot{\phi}_c \sim \frac{V}{Hv}$). On the other hand, ϕ_q represents quantum fluctuations of the scalar field in de Sitter space. These fluctuations result in the formation of a weakly inhomogeneous quasiclassical random field. After inflation ends, the Friedmann-Robertson-Walker horizon $\ell_c = 1/H$ grows and fluctuations with scales less than the horizon are smoothed out. Thus ℓ_c acts as an UV cutoff in the momentum distribution of this random field. In a spatial region of length l, the distribution of the fluctuations around ϑ can be calculated and is given by

$$P(\phi) = \frac{1}{\sqrt{2\pi}\sigma_\ell} \exp\left(-\frac{(\phi - \vartheta)^2}{2\sigma_\ell^2}\right), \quad (3)$$

where

$$\sigma_\ell^2 = \frac{H_i^2}{4\pi^2} \ln\left(\frac{\ell}{\ell_c}\right) \quad (4)$$

(and, as has been discussed in [13], for fields produced towards the end of inflation, one can ensure that the long-wavelength components in the Fourier decomposition of the random field ϕ_q do not introduce unacceptable for our discussion correlations between the values of the random field at distant points).

Clearly, such transitions can only occur in a system that is too weakly coupled to achieve thermal equilibrium. A number of such biased transitions have been investigated, including those occurring in very light scalar fields in de Sitter space [19].

The two disconnected minima are denoted by (+) and (−), respectively. At the phase transition, the field has some finite correlation length (like the inverse Ginzburg temperature in the case of a transition triggered by thermal fluctuations) over which the post-transition vacuum is chosen coherently, denoted by Λ. One can approximate the initial spatial structure of the vacuum produced during the transition by first dividing space into cells of volume Λ^d, where d is the dimension, and second, by assuming

that choices of the new vacua are made independently in each cell, giving the (+) vacuum with probability p and the (−) vacuum with probability $1 - p$, where $0 \leq p \leq 1/2$. Whenever the vacua in neighboring cells are different, a domain wall will form which interpolates between them, and so, typically, a complicated spatial network of domain walls will form.

Of course, an arbitrary spatial superposition of domain walls, such as that produced by the mechanism described above, is not a solution of the equations of motion and cannot be stable. However, such a superposition represents physical initial conditions, the subsequent evolution of which is governed by the dynamics of the theory. Subject to this dynamics, the initially static domain walls acquire nonzero velocities, oscillate under their surface tension, and interact with each other. This will be discussed in subsequent sections, where we will summarize the main ingredients, but also motivation and naturalness of out-of-equilibrium, biased phase transitions, where the bias can come from:

(i) small differences in the energy of the minima of the potential, and

(ii) different probabilities to reach these minima.

IV. DYNAMICS OF THE SCALAR FIELD AND WALL NETWORK

How do we study the behavior of a "biased network"? The scalar field is initialized by randomly setting it equal to $-\phi_0$ or $+\phi_0$ at each lattice site, with bias probability p for $+\phi_0$ and $1 - p$ for $-\phi_0$, with $0 \leq p \leq 1/2$. The lattice resolution corresponds to the initial field correlation length, and on physical scales above the resolution cutoff the field will have a white noise power spectrum (yielding results similar to percolation theory).

In this section, we follow the study presented in [8] and subsequently extended in [10]. The dynamics of the scalar field ϕ are determined by the equation of motion. This has the form

$$\frac{\partial^2 \phi}{\partial t^2} + \frac{3}{a}\frac{\partial a}{\partial t}\frac{\partial \phi}{\partial t} - \frac{1}{a^2}\nabla^2\phi = -\frac{\partial V}{\partial \phi}, \quad (5)$$

and, introducing the conformal time η (with $d\eta = \frac{dt}{a(t)}$), it becomes

$$\frac{\partial^2 \phi}{\partial \eta^2} + 2\frac{\partial a}{\partial t}\frac{\partial \phi}{\partial \eta} - \nabla^2\phi = -a^2\frac{\partial V}{\partial \phi}. \quad (6)$$

In the above, a is the scale factor of the Universe ($a \sim \eta$ in the radiation era, and $a \sim \eta^2$ in the matter era), V is the scalar potential and the spatial gradients are with respect to comoving coordinates. Then

$$\rho = \frac{1}{2}\frac{\partial^2 \phi}{\partial t^2} + \frac{1}{2a^2}|\nabla\phi|^2 + V(\phi), \quad (7)$$

$$p = \frac{1}{2}\frac{\partial^2 \phi}{\partial t^2} - \frac{1}{6a^2}|\nabla\phi|^2 - V(\phi). \tag{8}$$

The scalar potential determines the topology of the vacuum manifold. A typical choice is a ϕ^4 potential

$$V(\phi) = V_0\left(\frac{\phi^2}{\phi_0^2} - 1\right)^2 \tag{9}$$

with the two degenerate vacua $\phi = \pm\phi_0$ separated by a potential barrier V_0.

One can define a physical domain-wall thickness w_0 given by

$$w_0 \equiv \pi\frac{\phi_0}{\sqrt{2V_0}}. \tag{10}$$

The ratio of the wall thickness to the horizon size [$\mathcal{H}^{-1} = (\frac{1}{a}\frac{\partial a}{\partial \eta})^{-1}$] at the time of the phase transition

$$W_0 \equiv \frac{w_0}{a(\eta_0)}\frac{1}{\eta_0}\frac{d\ln a}{d\ln\eta}\bigg|_{\eta_0} \tag{11}$$

then sets η_0, the conformal time of the phase transition and the time at which we begin the simulation (one needs the walls to be thinner than the horizon in order to study their dynamics, namely, $w_0 \ll H^{-1}$).

Here we assume that the expansion is dominated by some smooth component, filling the Universe. The equation of state of this component is $p = \alpha\rho$. This gives $a(t) = a_0 t^{2/3(\alpha+1)}$, and $d\eta = \frac{dt}{a(t)}$, $\eta = t^{3\alpha+1/3(\alpha+1)}$. Also,

$$a(\eta) \sim \eta^{2/(3\alpha+1)} \sim \eta^\omega.$$

The equation of motion for static domain walls is [8]

$$\phi = \phi_0\tanh\left[\frac{\sqrt{2V_0}}{\phi_0}a(z - z_0)\right] \equiv \phi_0\tanh\left[\frac{a(z - z_0)}{w_0}\right] \tag{12}$$

and for nonstatic (boosted with a velocity v_0)

$$\phi = \phi_0\tanh\left[\frac{\gamma_0}{w_0}a(z - z_0 - v_0t)\right], \tag{13}$$

where $\gamma_0 \equiv (1 - a^2 v_0^2)^{-(1/2)}$.

The energy and surface density of the walls are

$$\rho(z) = \frac{\gamma_0^2 V_0}{2}\text{sech}^4\left[\frac{\gamma_0}{w_0}a(z - z_0 - v_0t)\right], \tag{14}$$

$$\sigma = a\int_{-\infty}^{+\infty}\rho(z)dz = \frac{2\gamma_0 V_0 w_0}{3}. \tag{15}$$

Finally, during the expansion, the velocity of the wall changes according to

$$\gamma(t)v(t) \sim a(t)^{-4}. \tag{16}$$

Let us now pass to runaway potentials, of the form

$$V(s) = \frac{1}{2s}(A(2s + N_1)e^{-(s/N_1)} - B(2s + N_2)e^{-(s/N_2)})^2.$$

In this case we do not have an analytic solution of the domain-wall type, interpolating between finite and runaway minima. However, we may still use the domain-wall language to describe the distribution of energy and topology of the vacuum. We shall call "domain walls" the nonequilibrium configurations which appear on the lattice as joining field values in neighboring lattice sites; then, we can identify the position of these generalized walls as the link between the lattice sites occupied by different vacua. In the case of the runaway vacuum, we shall simply determine whether a field value at a given site belongs to the classical domain of attraction of that vacuum.

To further develop an intuitive feeling about the evolution of the system, we shall define a domain-wall width, demanding that it should correspond to a distance in configuration space over which the field gradient is of the order of the potential energy of the local maximum that separates the vacua. In other words,

$$\Delta = \frac{|\phi_{\max} - \phi_{\min}|}{\sqrt{V(\phi_{\max}) - V(\phi_{\min})}},$$

where $\phi_{\max}$ denotes the position of the maximum separating the domains of attraction of the finite minimum $\phi_{\min}$ and of the runaway minimum ($\phi \to \infty$).

V. NUMERICAL PROCEDURE: DESCRIPTION AND TESTING

The numerical implementation of the equation of motion (6) is nontrivial. It involves discretization of the equation of motion (Appendix A), which allows treating the domain-wall network numerically. Moreover, the calculations are very time-consuming, unless an optimization of the time step is applied. We propose in Appendix B such a technique, which very significantly improves the efficiency of the code and allows us to go to larger lattices and higher accuracies. The role of the size of the lattice is discussed in Appendix C.

There are additional considerations to be made: To start with, the factor a^2 on the right-hand side of the equation of motion makes the effective potential barrier grow with the expansion. The result is that, in comoving coordinates, the width of the walls decreases like a^{-1}, which is η^{-1} for a radiation-dominated and η^{-2} for a matter-dominated universe. This implies that, on any reasonably sized grid, it is impossible to ensure that the walls would be visible on the lattice to the end of a calculation, when the horizon size is roughly the grid size. To appropriately represent walls, their width should be of the order of a few lattice sites during the whole simulation (in our case, we require the walls to be about five lattice sites wide since, if they become too wide, we lose the resolution).

However, we know that the dynamics of the walls do not depend on their width once they get created and separated from each other [8], and the same is true for the total surface energy and surface tension. As a result, one can consider a generalization of the equation of motion, which may force the walls to maintain a constant comoving thickness while otherwise not altering their dynamics. This modified equation is

$$\frac{\partial^2 \phi}{\partial \eta^2} + \frac{\alpha}{\eta}\left(\frac{d\ln a}{d\ln \eta}\right)\frac{\partial \phi}{\partial \eta} - \nabla^2 \phi = -a^\beta \frac{\partial V}{\partial \phi}, \qquad (17)$$

and, for $\alpha = \beta = 2$, we recover the initial equation of motion.

If $\beta = 0$, the walls will have constant comoving width. This choice does alter the scaling of the adiabatic effects of the Hubble expansion ($\beta = 0$), but this effect can be compensated by a proper choice of α. It turns out that [8]

$$\langle \phi - \phi_0 \rangle_{\text{rms}} \sim a^{-(\alpha/2)-(\beta/4)}. \qquad (18)$$

Thus, for $\beta = 0$, we have to set $\alpha = 3$ to have the same scaling of the deviation of ϕ and ϕ_0. In addition,

$$\gamma v \sim a^{-\alpha-(\beta/2)}. \qquad (19)$$

Having obtained a consistent set of equations, the next step is to understand the relevant range of initial conditions and parameters. As in previous works, we will set $\phi_0 = 1$. The scalar field initial conditions are then chosen using the prescription described above for various bias probabilities p. That is, in the following we will use percolation theory with allowed field values of ± 1 at any lattice site. It is of interest to compare the evolution of the network initialized with two-point initial conditions with those initialized with various continuous distributions. We have done this for a uniform distribution which gives probability $1 - p$ of choosing ϕ between -1 and 0 and probability p of choosing between 0 and 1, and with a Gaussian distribution $P(\phi)$ such that $\int_0^{+\infty} d\phi P(\phi) = p$. In general, the surface area of the initial network, measured at $\eta = \eta_0$, is larger in the case of the two-point, percolative distribution. However, after a few steps of dynamical evolution the network stabilizes, and its important characteristics, such as surface energy or kinetic energy and their time evolution, become indistinguishable for a fixed bias p. Hence, the sharp initial conditions of percolation theory also give a good approximation to initial conditions softened by smooth distribution functions. This justifies the use of the pure two-point percolation theory initial conditions in this paper.

We will set the initial field "velocity" $\dot{\phi}$ to be zero everywhere on the lattice (in previous work the results were found to be insensitive to small initial velocities with respect to the energy of the barrier [10]; this was done by repeated simulations with $\dot{\phi}$ chosen from a uniform distribution of velocities between -1 and $+1$ [$\sim \mathcal{O}(\phi_0/\eta_0)$]).

Simulations are run in the radiation-dominated epoch, with an initial time $\eta_0 = 1$, unless stated otherwise. We chose a wall thickness $w_0 = 5$ and a ratio $W_0 = 5$ [see (11)]. This value is used to ensure that the wall thickness is well above the lattice resolution scale (recall $\Delta x = 1$), while also ensuring that for most of the dynamical range of the simulation, the wall-wall separation exceeds the wall thickness.

We tested our code with the simplest case one can study, namely, the double-well potential, for which

$$V(\phi) = V_0 \left(\left(\frac{\phi}{\phi_0}\right)^2 - 1\right)^2$$

$[V(\phi) = m\phi^2 + \lambda\phi^4, m = -2V_0\phi_0^2, \lambda = V_0]$.

Looking at the potential and the first derivative (Fig. 2) we see that, while the potential is symmetric (even), the first derivative is asymmetric (odd):

This is a special situation, and this symmetry is violated in the case of the exponential potential discussed later on.

For the numerical part, we followed [8,10], setting the values of the parameters α and β to reproduce the original equation of motion, Eq. (6). In the runs the domain walls maintained a constant physical rather than comoving thickness, and so problems of available dynamic range become important. The prescription used is as follows: The simulation is run on a 512×512 lattice, with our standard field initial conditions and $p = 0.5$. Using a wall thickness of $w_0 = 25$, the initial conditions were evolved with the standard parameter values of $\alpha = 3$ and $\beta = 0$, until a time when the wall-wall separation exceeded the wall thickness, that is, a time $\eta = 2w_0$. The equation of motion was then changed, to set $\alpha = \beta = 2$ until a time $\eta = 250$. The comoving thickness of the walls at the end of the simulation was then 5 lattice sites. To compare, the run was repeated, this time leaving the standard parameter values fixed throughout the simulation.

Looking at the evolution of the energy density of the network of domain walls in three dimensions (in a radiation-dominated epoch), we confirm the following results [10].
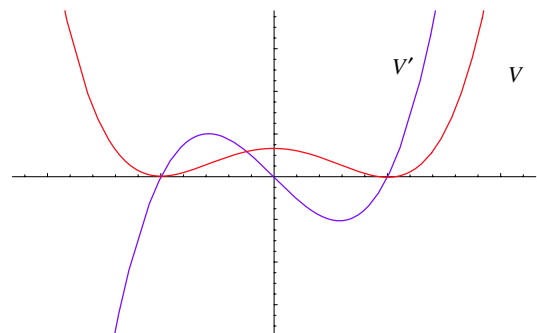

FIG. 2 (color online). Shape and first derivative of the double-well potential.

(i) For $p < 0.311$, the critical threshold of percolation theory, only one vacuum percolates the lattice, and isolated bags of one vacuum are to be found in a percolating sea of the more dominant vacuum. These bags rapidly decay under their surface tension.

(ii) For $0.5 > p > 0.311$, both vacua percolate, leading to an initial network of infinite (lattice-sized) domain walls. However, these also rapidly decompose into vacuum bags which then decay.

(iii) Only in the exact $p = 0.5$ case, long-term scaling that dominates the energy density of the Universe is found.

What is thus seen is that a network of domain walls forming well before matter-radiation equality can be sufficiently massive to contribute significantly to large scale structure formation on comoving scales less than ~ 20 Mpc. However, such a network will decay before photon decoupling.

An immediate question is whether superhorizon fluctuations can be of any relevance. In principle, such a possibility can arise, particularly in a universe with a significant hot dark matter component, and scale-invariant primordial perturbations induced by an earlier inflationary epoch. However, similarly to [10], we found that, for much of the range of biases, wall networks turned out to be cosmologically innocuous, as their energy density exponentially decays with a characteristic time of only a few expansion times. Simulations were made in both 3-dim and 2-dim; in the latter case walls stay around longer, but still, for any significant scaling of the network before the ultimate exponential decay, fine-tuning of p close to $1/2$ is required.

In principle, one has to also consider the possibility of having bias in the initial velocities. However, for the double-well potentials, modifications from such effects are negligible. The reason is that in this case the field is perfectly reflected to the minima by the external barriers; this however is not what happens for the runaway potentials that we will proceed to discuss, as well as for periodic potentials.

VI. BIASED POTENTIALS WITH NONDEGENERATE MINIMA

In the previous section, we summarized the expectations for potentials with degenerate minima. However, the behavior of domain walls can change radically in the case that the minima of the potential are unstable. Before studying the domain-wall dynamics that are to be expected, we would first like to discuss the naturalness of such solutions.

This problem has been studied extensively in [12], where specific realizations of such scenarios have been proposed: In realistic standard model extensions, and particularly in superstrings, there are usually several discrete groups Z_N. The fields in the theory then transform as α^r, $r = 0, 1, \ldots, N - 1$, where α is the Nth root of unity, and the effective potential is constructed from Z_N invariant

combinations of the fields. In nonsupersymmetric models, for example, the Lagrangian of a complex scalar field Φ transforming as α has the form:

$$L = \partial_\mu \Phi \partial^\mu \Phi^* + \mu^2 \mid \Phi \mid^2$$
$$- \frac{\lambda \mid \Phi \mid^4}{4} + \lambda' \left(\frac{\Phi^N}{M^{N-4}} + \frac{\Phi^{*N}}{M^{N-4}} \right) + \cdots, \quad (20)$$

where the coupling λ is made real by absorbing its phase in the field Φ. The coupling λ' is of order unity. The nonrenormalizable terms of dimension >4 arise because we have an effective field theory generated by physics at some (high) scale M.

If μ^2 is positive, the effective potential for Φ has a minimum for the nonvanishing value of the modulus and leads to spontaneous symmetry breaking of the discrete Z_N group. In this case it is convenient to reparametrize Φ as

$$\Phi = (\rho + v)e^{i\theta/v+\alpha}, \quad (21)$$

where $ve^{i\alpha}$ is the VEV (vacuum expectation value) of Φ, while ρ and θ are real scalar fields. The potential of the field θ is then [12]

$$V(\theta) = \frac{2\lambda' v^N}{M^{N-4}} \cos\left(\frac{\theta N}{v} + N\alpha \right) \quad (22)$$

and the value of the pseudo-Goldstone mass is given by

$$m^2 = \frac{N^2 V_0}{v^2} \cos(N\alpha), \qquad V_0 \equiv \lambda' \frac{2v^N}{M^{N-4}}. \quad (23)$$

The potential of Eq. (22) has an N-fold degeneracy corresponding to $\theta/v \rightarrow \theta/v + 2\pi/N$.[1]

How can this degeneracy be lifted? So far we have discussed domain walls which are expected to arise from the potential of a *single* scalar field Φ. However additional scalar fields are also present. Then, if, as is likely, the interactions between the fields cause more than one field transforming nontrivially under the discrete symmetry group to acquire a VEV, it is possible to generate a situation in which the vacuum degeneracy is apparently lifted: If one of these fields acquires its VEV before or during inflation, the observable universe will have a unique value for its VEV. After inflation the effective potential describing the remaining fields may still have an *approximate* discrete symmetry, but the vacua will not be exactly degenerate.

To illustrate this, for instance in nonsupersymmetric models, consider adding to the above theories a second field Φ'. If Φ transforms as α^m and Φ' as α^n under the symmetry group and assuming that $n \geq m$ and N/n is integer in order to simplify the analysis, the potential is [12]

---

[1]Pseudo-Goldstone bosons, due to their very light mass and negligible interactions, may very naturally give rise to late phase transitions [20].

$$V(\theta) = \sum_{r=0}^{N/n} \left[2 \frac{v^{(N-nr)/m} v'^r}{M^{(N-(n-m)r)/m-4}} \right.$$
$$\left. \times \cos\left(\frac{r\theta'}{v'} + \frac{(N-nr)}{m}\alpha + r\beta \right) \right]. \quad (24)$$

Clearly there will be a dominant term; however, the subdominant ones will *slightly* split the degeneracy of the potential.

Having summarized the model building aspects, the next question is whether the domain walls to be expected in these theories can be of any relevance for structure formation.

In the case of nondegenerate minima, we expect that there is a critical scale at which the loss in surface energy from collapsing horizon-size bubbles becomes similar to the gain in volume energy by passing to the true minimum. At some stage, the true minimum will be favored at all horizons, and walls will disappear. In this case, for sub-horizon fluctuations, we will have a maximum scale, corresponding to the size of the horizon R at the time that the walls disappear (which today would correspond to $R' = R_{H_0}/\sqrt{1+z_a}$). These could in principle generate structure for the smaller angular scales of WMAP. The question of course is what the situation is regarding superhorizon fluctuations, and whether these can give any structure at the largest scales (Cosmic Background Explorer and the largest scales of WMAP).

The time when walls disappear is specified by a redshift z_a, which is a calculable quantity, even before passing to any numerical simulation. For nondegenerate vacua there is always a critical bubble radius above which it is energetically favorable for the bubble of true vacua to expand gaining more volume energy than is lost in surface energy. Once the horizon exceeds this critical radius, bubbles of the true vacuum will expand everywhere at the speed of light to fill the whole universe and this occurs at the same time in all horizon volumes [21]. Then, the nondegeneracy of the potential is measured by a factor $\delta\rho \approx \frac{\sigma}{R}$. For instance, if walls decay during matter dominance, this determines the redshift z_a to be

$$z_a = \left(\frac{\delta\rho R_{H_o}}{\sigma} \right)^{2/3} - 1. \quad (25)$$

In what follows, we combine biasing with nondegeneracy of minima, a situation that, according to the above, can arise for effective potentials generated by several weakly interacting scalar fields. Then, if the minimum with the highest probability has a higher energy than the second one, we have two competing effects, which can allow modifications from previous results in the literature. This is illustrated in Fig. 3.

To understand these effects, we perform a numerical simulation. A simple and generic parametrization of the nondegeneracy of the potential is obtained by adding to
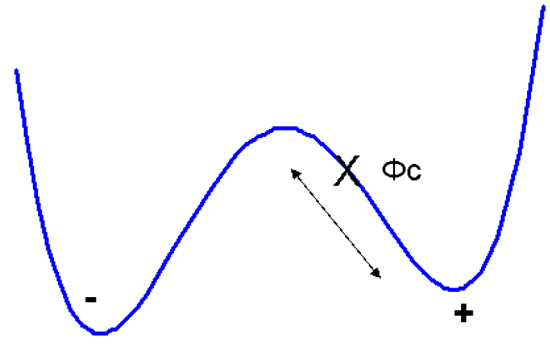

FIG. 3 (color online). Schematic illustration of biased, out-of-equilibrium phase transition, in a potential with nondegenerate minima. The field is shifted towards the false vacuum.

$V(\phi)$ a term linear in ϕ, namely,

$$V(\phi) \to V(\phi) - \epsilon V_0 \phi.$$

The monitoring of the extrema of the potential is shown in Appendix D. During the evolution, the field "feels" only the derivative of the potential and the gradient of the field, and thus it has the tendency to evolve towards the place where the magnitude of the derivative is larger. This may in principle compensate the biasing of the initial distribution; in fact, the two effects can be combined in a way that one produces a quasistable network, which is shown in Fig. 4.

In the upper panel of Fig. 4, we present the evolution of the surface energy of the walls as a function of the conformal time η, for three different cases with the bias in the initial distribution corresponding to $p_- = 0.47$:

(i) The upper curve (a) corresponds to the case where the effect of the nondegeneracy of the minima, parametrized by $\epsilon = -0.012$, is partially cancelled by the bias in the initial field distribution.

(ii) The middle curve (b) stands for the case of degenerate minima.

(iii) The lower curve (c) denotes the case with a higher nondegeneracy of the minima, parametrized by $\epsilon = -0.02$. As expected, this choice leads to a rapid disappearance of the walls.

The middle picture shows the behavior of the surface energy of the network for different initial distributions and a fixed value of the nondegeneracy of the minima ($\epsilon = -0.012$).

(i) Curve (a) is the same as above, with a bias given by $p_- = 0.47$.

(ii) Curve (d) corresponds to a bias $p_- = 0.39$, that is a probability to occupy the left (lower) vacuum equal to 0.39.

In curves (b) and (c) the initial bias of the distribution is given by $p_- = 0.46$ and $p_- = 0.44$, respectively. In these cases the offset has been tuned in such a way that it compensates the effect of nondegeneracy. One should note that the necessary tuning is of the order of a few
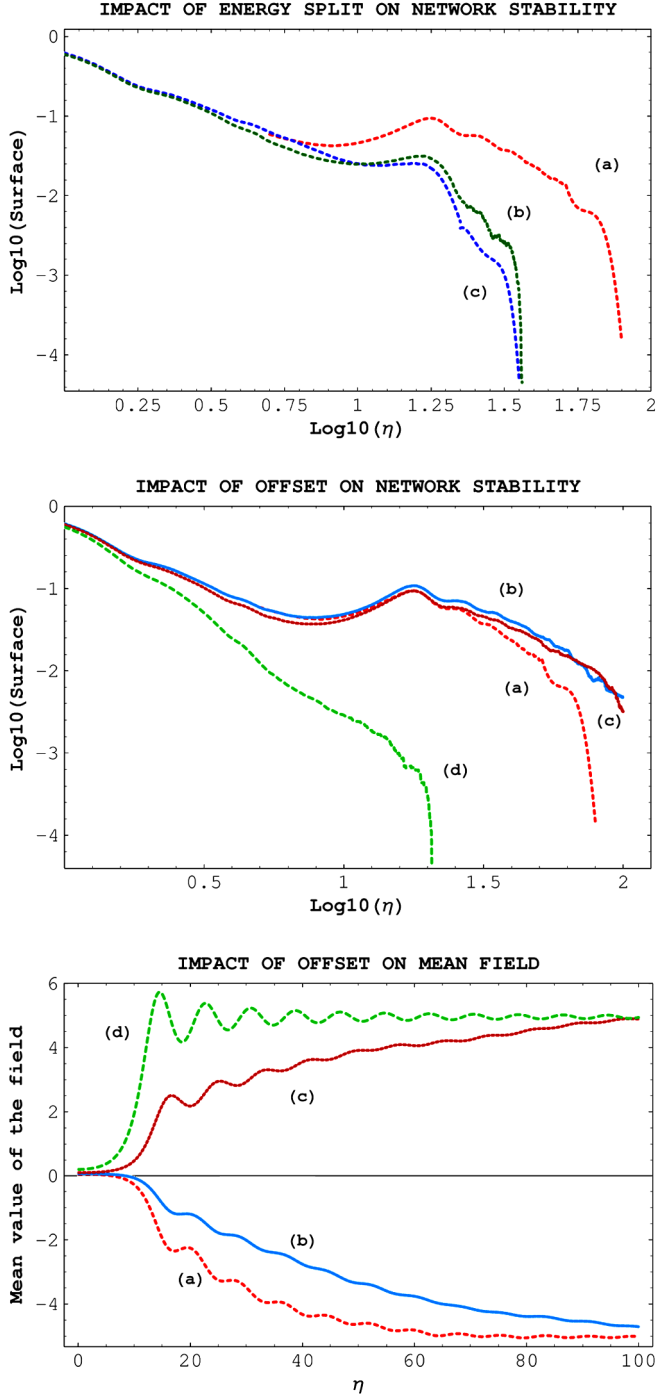
FIG. 4 (color online). Domain-wall evolution in potentials with nondegenerate minima and a bias in the initial mean field distribution.

TABLE I. Fit of the wall surface area as a function of the conformal time η-η_0, for different values of the nondegeneracy of the minima ϵ and for $p = 0.47$ (upper panel of Fig. 4).

Curve	Split ϵ	$\bar{\nu}$	$\bar{\eta}$
(a)	-0.012	-0.367	-35.81
(b)	0	-0.2	-13.37
(c)	-0.02	0.06	-9.79

TABLE II. Fit of the wall surface area as a function of the conformal time η-η_0, for different values of the probability p and for a fixed nondegeneracy of the minima $\epsilon = -0.012$ (middle panel of Fig. 4).

Curve	p	$\bar{\nu}$	$\bar{\eta}$
(a)	0.47	-0.367	-35.81
(b)	0.46	-0.626	-93.80
(c)	0.44	-0.72	-115
(d)	0.39	-1.86	-19.96

To capture quantitatively the scaling or no-scaling behavior of the networks, we have performed in each case the numerical fit of the surface area of the network as a function of the conformal time, according to the formula

$$A \sim \eta^{\bar{\nu}} 10^{\eta/\bar{\eta}}. \tag{26}$$

Each curve has been fitted over the time intervals after the initial period of numerical ''unequilibrium,'' which ends approximately at the position of the characteristic peak located near $\log_{10}(\eta_{eq}) = 1.3$.

In Table I, we give the values of $\bar{\eta}$ and $\bar{\nu}$ corresponding to the upper panel of Fig. 4. In Table II, we give the values corresponding to the curves from the middle panel of Fig. 4. The cases with a large magnitude of $\bar{\eta}$ correspond to quasiscaling networks, with powers of the slow, power-like, decay given by the respective values of $\bar{\nu}$. The networks showing such a behavior are represented by curve (a) in Table I and curves (b) and (c) in Table II. In the remaining cases the predominant behavior is that of the exponential decay with relatively small decay constants (i.e. lifetimes). The values of $\bar{\nu}$, being related to small corrections to the exponential behavior, are only indicative, and are given for the sake of comparison.

The outcome is that we were able to realize a quasistable wall network by combining two competing effects.

VII. RUNAWAY POTENTIALS

A. Theoretical motivation and description of the potential

Runaway potentials arise commonly in theories of dynamical supersymmetry breaking, and hence their collective dynamical properties deserve a careful study. For the purpose of this paper we assume the potential in the form
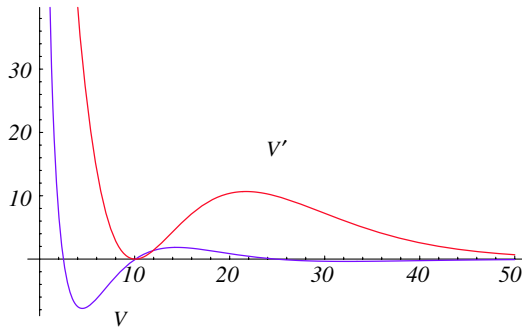
percent, enhancing the *a priori* probability of occupying the right vacuum by about 5%.

The lower panel shows the evolution of the mean value of the scalar field during the decay of the wall network, for the same choice of parameters as in the middle panel. Curves (a)–(d) correspond to the respective ones in the middle panel.

FIG. 5 (color online). Shape and first derivative for the runaway potential.

$$V(s) = \frac{1}{2s}(A(2s + N_1)e^{-(s/N_1)} - B(2s + N_2)e^{-(s/N_2)})^2.$$

Its shape and first derivative are plotted in Fig. 5.

If we would like to identify the field s with a stringy modulus, say, a dilaton, then we would have to define $s = e^{\sqrt{2}\phi}$, so that ϕ is canonically normalized. This makes the above potential a doubly exponential function of ϕ. However, in what follows we shall simply assume that the Kähler potential for s is canonical; this simplification does not introduce qualitatively new features in the simulations. In general, one can see that the doubly exponential steepness of the potential makes the evolution more sensitive to the changes of the offset and the width of the distribution.

The degeneracy of this potential can be lifted by adding a term of the form $\frac{\epsilon}{s^2}$. The position of the extrema of the potential and the way they are monitored in our simulations are discussed in Appendix D.

We have studied runaway potentials for the parameter set of Table III, which corresponds to a weakly coupled vacuum. The expectation value of s ($\langle s \rangle \sim 10$) corresponds to the inverse square of a gauge coupling in a supersymmetric Yang-Mills theory.

In Table III, min and max denote the minimum and maximum, respectively, of the potential, and w_0 gives the width of the (approximate) domain wall. The initial conditions are controlled by the position of the mean value of the initial distribution $\langle \phi \rangle = \text{max} + w_0\gamma$ and by the initial width of distribution $\sigma_\phi = w_0\gamma'$, where γ, γ' are real numbers.

B. Numerical simulations for runaway potentials

Runaway potentials are in principle more complicated to study than the double-well ones, since they have more intrinsic instabilities. This implies that several of the assumptions made for the simplest potentials have to be reconsidered. This by itself is an interesting problem and will allow us to understand the level of validity of the results in potentials that are to be expected in theoretically motivated models.

### *1. Modification of equation of motion*

The first step is to analyze what the effect is of the modification of the equations of motion (by taking $\alpha = 3$ and $\beta = 0$), in order to maintain a constant comoving thickness for the walls, while maintaining the condition for conservation of the wall momentum, namely, $\beta = 6 - 2\alpha$.

To do so, we perform simulations for intermediate values of α and β to see how this modification changes the evolution of the wall network. The results are shown in Fig. 6.

In general, the larger β is, the slower is the rate of disappearance of the false vacuum. When $\beta > 1.2$, the bubbles of the vacua become stable. This is because the effective potential barrier grows with time with respect to the gradients, so they cannot overcome the potential. When $\beta < 1.2$, the pressure of the dominant vacuum takes over.

2. Study of the equation of state

As discussed in previous sections, we assume that the expansion of the Universe is dominated by some smooth component, filling the Universe. Then, if we go smoothly
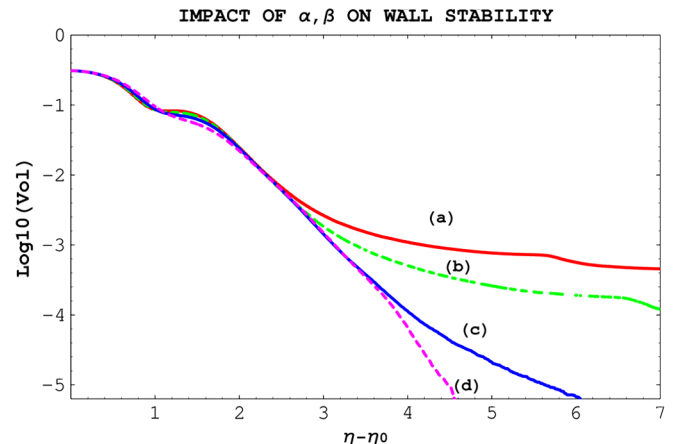
	(a)	(b)	(c)	(d)
α	1.8	2.0	2.4	3.0
β	2.4	2.0	1.2	0.0

FIG. 6 (color online). $\log_{10}(\text{Vol}(L))$ as a function of $\eta - \eta_{\text{start}}$, for four different combinations of α and β.

TABLE III. Runaway potential parameter set used in our simulations.

A	B	N_1	N_2	min	max	w_0
1.0330	1.1950	10.0	9.0	10.075	21.729	3.567

between dust ($\alpha = 0$) and radiation ($\alpha = 1/3$), the parameter ω changes from 2 to 1. We made simulations for various values of ω, to see whether this influences the evolution. The results are shown in Fig. 7.

We see that all the measured observables change smoothly with ω and are not influenced very much. In general, the faster the scale factor $a(\eta)$ grows, the slower the walls disappear.

3. Role of the horizon at the time of network creation

If the scale factor behaves like $\alpha(\eta) \sim \eta^\omega$, the horizon (inverse Hubble constant) grows with time as $H^{-1} = \frac{\eta^{\omega+1}}{\omega}$. Hence, different values of η_{start} give different values of the horizon at the point of the phase transition. The results should be sensitive to that, and, to test how the evolution of the field changes with the change of the initial horizon, we performed several simulations for η_{start} changing between 10^{-4} and 10 (in almost all published simulations this parameter was taken to be 1). The results are given in Fig. 8.
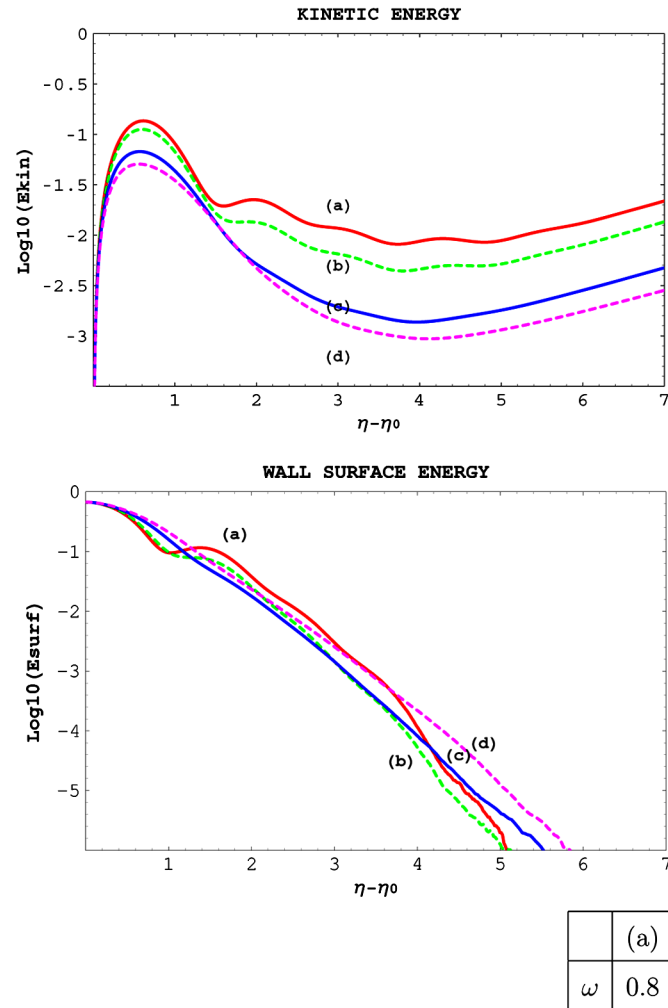

IMPACT OF η_0 ON WALL STABILITY

	(a)	(b)	(c)	(d)
η_{start}	10.0	5.0	0.8	10^{-4}

FIG. 8 (color online). $\log_{10}(\text{Vol}(L))$ versus $\eta - \eta_{start}$ for different values of η_0.

KINETIC ENERGY

WALL KINETIC ENERGY

WALL SURFACE ENERGY

VOLUME OF LEFT VACUUM

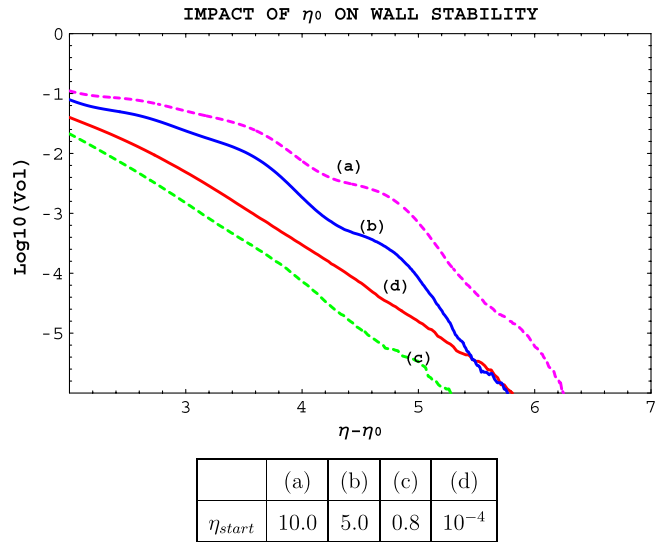|	(a)	(b)	(c)	(d)
ω	0.8	1.0	1.6	2.0

FIG. 7 (color online). $\log_{10}(\text{Vol}(L))$ versus $\eta - \eta_{start}$ for different values of ω.

Figure 8 indicates the existence of two competing effects:

(i) For very small values of η_{start}, the horizon is much smaller than the wall width. Then, the friction term in the equation of motion is large and temporarily freezes the evolution of the network. One can see that for $\eta_{\text{start}} = 0.8$ the network is less stable than for $\eta_{\text{start}} = 10^{-4}$—in the first case the wall width-to-horizon ratio is smaller than in the second, and walls evolve faster under the influence of the potential; consequently the surface of walls decays faster.

(ii) However, for large values of η_{start}, corresponding to curves (a) and (b), many walls fit within the horizon and interactions between walls, of the joining and splitting type, become important and tend to stabilize the network. This is illustrated by the fact that the network corresponding to $\eta_{\text{start}} = 10$ is more stable than the one for $\eta_{\text{start}} = 5$, as in the first case there are more walls inside the horizon.

One should note that, at the initial stage of the evolution, in the cases where the horizon is large, there is a period when the domain-wall surface grows with time.

C. Nearly scaling solutions for runaway potentials

The dynamics of the walls are determined by several parameters: the distance to the horizon at the time the evolution starts $H^{-1} = \eta^{\omega+1}/\omega$, the width of the wall Δ, the width of the initial distribution σ and the offset of the initial distribution with respect to the maximum of the potential $\bar{\phi} = \phi_{\text{mean}} - \phi_{\text{max}}$. Independently of the absolute positions of the extrema and of the absolute height of the maximum of the potential, the relations between these parameters shall determine the behavior of the system.

1. Width of the walls

The domain-wall width is defined as

$$w_0 = \frac{\text{width of barrier}}{\sqrt{\text{height of barrier}}}.$$

In our simulations, the width of the barrier is numerically constant and the width of the walls will change by changing the height of the barrier. We have performed simulations, to check how the width of the walls influences their evolution, for a range of w_0 between 0.05 and 20.0 lattice sites.

These indicate that, if the walls are thin, their evolution is dominated by the potential energy, and field gradients are almost unimportant (in each site of the lattice the field evolves independently of the other site, so, effectively, the walls become frozen in). In this case the overall behavior of the field, as measured by the time dependence of the mean value, is rather classical. The wider the walls, the milder the influence of the potential; gradients contribute significantly to the dynamics, and the evolution of the mean value of the field becomes nonclassical. If the walls

are wide, between 2 and 20 lattice sites, the evolution is insensitive to the domain-wall width.

2. Initial width of the distribution

In the runs presented in this paper the field has been initialized randomly, according to a Gaussian distribution. The larger the width of the distribution, the larger the probability to create many walls. Hence, if we initialize according to a wider distribution the network lasts longer, meaning that for wider distribution, it matters less where the center of the distribution is (the biasing becomes less important, since the field can climb over the barrier with a higher probability). This is particularly significant for the runaway potential, which is asymmetric, since the potential force (derivative) to the left of the barrier is larger than the one to the right. As a result, at some stage the false vacuum (the finite one) starts growing, because the force towards the left vacuum is somewhat larger.

3. Initial mean value of the field

We have performed simulations for various positions of the center of the distribution for the runaway potential. If the field starts to the left of the maximum, even high above the barrier, then, very often, the whole space finishes in the false vacuum. The reason is the asymmetry of the force in this potential, together with the damping due to the Hubble expansion (and the fact that the friction term is proportional to the time derivative of the field, which may be large in such situations). Most interesting effects are seen when the initial value of the field is close to the maximum—then we get plenty of walls which disappear rather slowly. If we want to obtain a stable network, then we have to start slightly to the right of the maximum, again because of the asymmetry of the force. In these cases the networks exhibit nearly scaling behavior.

4. Examples of nearly scaling networks

The advertised behavior has been illustrated in Fig. 9. No splitting term has been switched on in this case.

(i) Here, curves (a) and (b) correspond to initial distributions positioned at the top of the barrier and different widths [1.5 domain-wall width for curve (a) and a single domain-wall width for (b)]. In both cases the field evolves towards the left vacuum, with the difference in the widths playing a minor role.

(ii) Curves (c) and (d) correspond to the initial mean value of the distribution, shifted by one-twentieth of the wall width to the right of the top of the potential and width of the distribution equal to 1.5 domain-wall width for (c), and to the domain-wall width for (d).

Again, to capture quantitatively the scaling behavior of the networks, we have performed the numerical fits of the
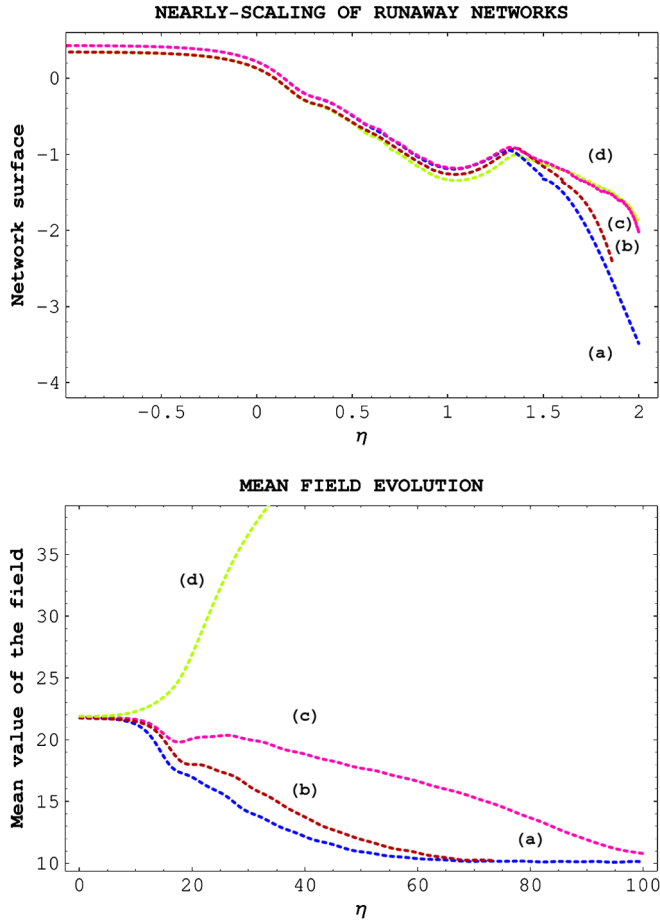
FIG. 9 (color online). Wall network evolution in runaway potentials.

surface area of the networks as functions of the conformal time, according to the formula $A \sim \eta^{\bar{\nu}} 10^{\eta/\bar{\eta}}$. Each curve has been fitted over the time intervals after the initial period of numerical unequilibrium, which ends approximately at the position of the characteristic peak located near $\log_{10}(\eta_{eq}) = 1.4$. The results are shown in Table IV. The values of $\bar{\eta}$ and $\bar{\nu}$ given in this table correspond to the upper panel of Fig. 9. The cases (c) and (d) with the large magnitude of $\bar{\eta}$ correspond to scaling networks, with powers of the slow, powerlike, decay given by the respective values of $\bar{\nu}$. In the remaining cases (a) and (b) the predominant behavior is that of the exponential decay with

TABLE IV. Fit of the wall surface area as a function of the conformal time η-η_0, for runaway potentials, for the initial mean values of the distribution of the upper panel of Fig. 9.

Curve	$\bar{\nu}$	$\bar{\eta}$
(a)	-0.172	-31.45
(b)	-0.33	-48.42
(c)	-0.66	-242.10
(d)	-0.659	-231.61

relatively small decay constants (i.e. lifetimes). As in the case of the double-well potential, the values of $\bar{\nu}$ for (a) and (b) (related to small corrections to the exponential behavior) are only indicative and are given for the sake of comparison.

In both cases one observes a scaling behavior of the network surface; however, in the case of a wider initial distribution, the mean field behaves nonclassically and returns to the left vacuum, so eventually the left vacuum prevails over the runaway behavior.

To summarize, the asymmetry of the potential and its derivatives with respect to its maximum makes the evolution of broad and biased distributions nonclassical. In the limit of vanishing width of the distribution the classical behavior is recovered, which is a good check of the numerical routine. A wide class of initial distributions leads to a relatively short period with domain-wall networks, which however disappear rather quickly, leaving behind a system rolling towards infinity. This is a version of the Steinhardt-Brustein effect. However, a larger width of the distributions slows down the decay of the islands of "finite" vacua. As in the case of the symmetric double-well potential, the less favored vacuum assumes the topology of compact clusters submerged in the sea of the runaway vacuum. The formation of a pseudoinfinite cluster requires a higher degree of fine-tuning than in the case of the double-well potential. An important factor is the ratio of the distance to the horizon and the domain-wall width at the time when the initial conditions are imposed; if this ratio is truly small, the disappearance of the walls becomes slower. This is more or less expected, as in this case the cosmic friction term is able to compete efficiently with the potential force. In the simulations shown in the figures, we were assuming the initial horizon to be $H_i^{-1} = 10^{-4}$, which corresponds to walls much wider than the initial horizon. The small ratio discussed above can be obtained by making the phase transition occur shortly before the end of inflation, as discussed earlier in this paper.

VIII. CONCLUSIONS

The formation of large scale structure in the Universe is at present one of the most important areas where particle physics meets cosmology. In particular, important contributions to structure formation may come from phase transitions, especially when the mass order parameter is so small that the characteristic scale $1/m$ corresponds to the range of scales relevant for cosmological observations. It is also possible that the mass of the order parameters lies in the electroweak range, but the phase transition could be seen via its indirect effects. This is the case for the transition associated to supersymmetry breaking.

In the present work, using numerical and analytical methods, we studied the physics of the domain walls that appear during such phase transitions. In particular, we have investigated domain-wall networks and their evolution, for

two types of potential, and two ways of modeling the initial conditions after the phase transition. One of the potentials is the well-known double-well potential, and the second is the exponential potential, characteristic of supersymmetry breaking via gaugino condensation. In both cases, we checked the evolution of domain walls as a function of the parameters of the potential, in particular: (i) as a function of the nondegeneracy of the available vacua and (ii) as a function of a difference of probabilities of filling these vacua. To this end, we have constructed a C + + computing code, which we used to confirm earlier results and to extend our considerations to the new cases.

The program has been optimized, and we have found a theoretical estimate for the accuracy of the integration procedure. The latter is constantly monitored in order to enable the use of an adaptive time step that greatly increases the speed of the code while maintaining high sensitivity. Moreover, we investigated the role of the modifications of the equation of motion used to model the evolution on the grid.

The simulations show compensation effects between the nondegeneracy of the vacua and the asymmetry of the probability distribution: These competing effects may cancel each other, resulting in the creation of slowly disappearing metastable domain-wall networks, in very general and physically interesting situations.

Extensions to other types of potentials, as well as a detailed study of structure formation within this framework, shall be addressed in a separate publication.

ACKNOWLEDGMENTS

APPENDIX A: DISCRETIZATION OF EQUATION OF MOTION

In order to treat the equations of motion of the scalar field and the domain-wall network numerically, we divide the Universe into balls of radius ℓ much larger than H^{-1}, thus covering many Hubble horizons. We will then simulate the evolution of the network in a single ball of radius L. The lattice site at the beginning of the simulation corresponds to a single Hubble horizon. Moreover, we introduce multitorus topology of the grid (namely, periodic boundary conditions). To discretize the relevant equations, we use the "staggered leapfrog" method for the second-order time derivatives and the Crank-Nicholson scheme for spacelike derivatives. This means that we have second-order accu-

racy in differentials with respect to time and space. The discretized equations are as follows:

$$\delta = \frac{1}{2}\alpha\frac{\Delta\eta}{\eta}\frac{d\ln a}{d\ln\eta},$$

$$(\nabla^2\phi)_{i,j,k} \equiv \phi_{i-1,j,k} + \phi_{i+1,j,k} + \phi_{i,j-1,k} + \phi_{i,j+1,k}$$
$$+ \phi_{i,j,k-1} + \phi_{i,j,k+1} - 6\phi_{i,j,k},$$

$$\dot{\phi}_{i,j,k}^{n+(1/2)} = \frac{(1-\delta)\dot{\phi}_{i,j,k}^{n-(1/2)} + \Delta\eta(\nabla^2\phi_{i,j,k}^n - a^\beta\frac{\partial V}{\partial\phi_{i,j,k}^n})}{1+\delta},$$

$$\phi_{i,j,k}^{n+1} = \phi_{i,j,k}^n + \Delta\eta\dot{\phi}_{i,j,k}^{n+(1/2)}, \qquad (A1)$$

where $\eta = \eta_0 + m\Delta\eta$ (in the above, upper indices denote time steps and lower ones coordinates x, y and z). For clarity

$$\phi_{i,j,k}^n \equiv \phi(\eta', x', y', z'), \qquad \dot{\phi}_{i,j,k}^{n+(1/2)} \equiv \frac{\partial\phi}{\partial\eta}(\eta'', x', y', z'),$$

$$\frac{\partial V}{\partial\phi_{i,j,k}^n} \equiv \frac{\partial V}{\partial\phi}(\phi_{i,j,k}^n), \qquad x' = x_0 + i, \qquad y' = y_0 + j,$$

$$z' = z_0 + k, \qquad \eta' = \eta_0 + n\Delta\eta,$$

$$\eta'' = \eta_0 + (n + \tfrac{1}{2})\Delta\eta.$$

Here, $\dot{\phi} \equiv \frac{\partial\phi}{\partial\eta}$ and $x_0 = y_0 = z_0 = 0$.

For the mean value and the dispersion of the field, we have the following equations:

$$\mathrm{VOL} = N_x \cdot N_y \cdot N_z,$$

$$\langle\phi\rangle = \sum_{i,j,k}\frac{\phi(i,j,k)}{N_xN_yN_z} = \frac{\sum\phi}{\mathrm{VOL}},$$

$$\sigma_\phi^2 = \langle(\phi - \langle\phi\rangle)^2\rangle = \langle\phi^2\rangle - \langle\phi\rangle^2,$$

$$\frac{\sigma_\phi}{\langle\phi\rangle} = \frac{\sqrt{\frac{\sum\phi^2}{\mathrm{VOL}} - \langle\phi\rangle^2}}{\langle\phi\rangle}, \qquad \langle\phi^2\rangle = \frac{\sum\phi(i,j,k)^2}{\mathrm{VOL}}.$$

The kinetic energy is given by

$$E_{\mathrm{kin}} = \frac{\sum\dot{\phi}^2}{\mathrm{VOL}}.$$

In all simulations we assume that the field was initially at rest ($\Phi' = 0$), while for the surface energy we have

$$A = \int\vec{n}\cdot d\vec{A} = \Delta A\sum_{\mathrm{links}}\frac{\delta^\pm}{|\cos\theta_x| + |\cos\theta_y| + |\cos\theta_z|}$$
$$(A2)$$

$$= \Delta A\sum_{\mathrm{links}}\frac{\delta^\pm}{|n_x| + |n_y| + |n_z|} \qquad (A3)$$

$$= \Delta A \sum_{\text{links}} \frac{|\nabla \phi|}{|\frac{\partial \phi}{\partial x}| + |\frac{\partial \phi}{\partial y}| + |\frac{\partial \phi}{\partial z}|}, \qquad \text{(A4)}$$

$$\delta^{\pm} = \begin{cases} 1 & \text{if a link crosses a wall,} \\ 0 & \text{if it does not.} \end{cases} \qquad \text{(A5)}$$

$E_{\text{surf}} = \sigma A$, where σ is the tension and A the surface. In what follows, we take $\sigma = 1$ and

$$E_{\text{surf}} = \frac{A}{\text{VOL}}.$$

The kinetic energy of the walls is given by

$$E_{\text{kw}} = \sum_{\text{links}} \frac{1}{2}[\dot{\phi}(\vec{x})^2 + \dot{\phi}(\vec{x} + \vec{n})^2]$$

(with $\dot{\phi}$ computed at the position of the wall). To calculate the volume of the vacuum, we normalize to the total volume, namely, take the number of left vacua and right vacua over the total number of vacua.

In our code, instead of looking for the extrema of the potential analytically, we use numerical methods which are simpler (particularly for runaway potentials):

$$\frac{dV}{d\phi}(\phi) = \frac{V(\phi + \epsilon) - V(\phi - \epsilon)}{2\epsilon},$$

and we take $\epsilon = 10^{-4}$. The accuracy is $\epsilon^2 \frac{d^2 V}{d\phi^2}$.

APPENDIX B: TECHNICAL DISCUSSION ABOUT OPTIMIZATION OF SIZE OF TIME STEP

The basic parameter that determines the accuracy of the simulation is the time step, which must be small, so that the discretized equation must well represent the continuous one. However, the time step cannot be too small, because there are many steps in the integration and numerical mistakes accumulate (each step introduces an error).

We have seen that the field changes rapidly at the beginning of the simulation, which is due to the random, nonequilibrium initialization and somewhat later by the fact that domain walls get created rapidly and then interact very often (since there are many of them). After some time, the field changes at a slower rate, and its configuration becomes more regular and more stable. Consequently, we should change at some point the time step of the simulation (smaller one at the beginning, when the evolution is rapid, and larger, at later times).

The change of the field depends on the time step, and on the value of the time derivative in the next integration step

$$\Delta \phi = \Delta \eta \dot{\phi}.$$

Now, let us look at the evolution of the time derivative. The change of the time derivative over the time $\delta \eta$ is

$$\Delta \dot{\phi} \equiv \dot{\phi} - \frac{(1 - \delta)\dot{\phi} + \Delta \eta(\nabla^2 \phi - a^{\beta} \frac{\partial V}{\partial \phi})}{1 + \delta},$$

which gives

$$\Delta \dot{\phi} = \frac{1}{1 + \delta}[-2\delta \dot{\phi} + \Delta \eta(\nabla^2 \phi - a^{\beta} V')].$$

The parameter δ is given by

$$\delta = \frac{1}{2} \alpha \frac{\Delta \eta}{\eta} \frac{d \ln a}{d \ln \eta}.$$

Since $\alpha \sim 2$, and $\frac{d \ln a}{d \ln \eta} \sim 1$,

$$\delta \sim \frac{\Delta \eta}{\eta}, \quad \text{so} \quad \frac{1}{1 + \delta} \sim 1 - \frac{\Delta \eta}{\eta}.$$

Substituting, we get

$$\Delta \dot{\phi} \sim \Delta \eta \left[-2 \frac{\dot{\phi}}{\eta} + \nabla^2 \phi - a^{\beta} V' \right] \left(1 - \frac{\Delta \eta}{\eta} \right).$$

The expression in the square brackets can be estimated from above, by its largest value, taken anywhere in the lattice:

$$|\Delta \dot{\phi}| \leq \Delta \eta \left(\frac{-2|\dot{\phi}|_{\text{max}}}{\eta} + |\nabla^2 \phi|_{\text{max}} + |a^{\beta} V'|_{\text{max}} \right). \qquad \text{(B1)}$$

Now, we can follow several strategies:
(i) demand that the change to the field is as small as possible

$$\frac{\Delta \phi}{\phi} \ll 1,$$

(ii) demand that the average change of the field on the whole lattice should be smaller than 1

$$\left\langle \frac{\Delta \phi}{\phi} \right\rangle \ll 1,$$

(iii) request that the maximal change of the field with respect to the wall width is much smaller than 1

$$\frac{\Delta \phi}{w_0} \ll 1.$$

In our simulation, we have followed the last path, and thus

$$\frac{\Delta \phi}{w_0} \leq \kappa,$$

where κ is the requested accuracy. From this inequality, it turns out that

$$\Delta \eta = \sqrt{\frac{\kappa w_0}{\frac{-2|\dot{\phi}|_{\text{max}}}{\eta} + |\nabla^2 \phi|_{\text{max}} + |a^{\beta} V'|_{\text{max}}}}.$$

This is the estimated optimal time step.

To fix the optimal accuracy, we have performed several simulations, looking for the change of the results with

TABLE V. $(\Delta\eta)_{\min}$ versus κ.

κ	10^{-1}	10^{-2}	10^{-3}	10^{-4}	10^{-5}	10^{-6}
$(\Delta\eta)_{\min}$	1.85×10^{-1}	5.89×10^{-2}	1.79×10^{-2}	5.72×10^{-3}	1.85×10^{-3}	5.87×10^{-4}
$(\Delta\eta)_{\max}$	6.16×10^{-1}	2.03×10^{-1}	6.41×10^{-2}	2.02×10^{-2}	6.45×10^{-3}	2.09×10^{-3}

respect to changes of κ. We used a 2D lattice with a size of 248×248, for $w_0 = 356$. We also made a simulation on a larger lattice, 3072×3072, to understand the dependence on the lattice size. The results appear in Table V below.

It turns out that the kinetic energy, mean value of field and dispersion of the field are not sensitive to the time step; however, the surface energy, surface of walls and volume of different vacua are much more dependent on it (in fact, the most sensitive statistical observable is the ratio of the surface of the walls over the volume of the subdominant vacuum—namely, the rate of change of the volume of the walls).

In the simulations described so far in the literature, there is no analysis of the accuracy of the results, and the time step is usually not given. Instead, large series of simulations are performed and the results are averaged. However, it may be that the numerical noise is being averaged as well. The new element arising from our simulation is that, with an appropriately chosen time step, the plots of the parameters are similar for different runs, which makes them more reliable.

In our procedure, we first chose the optimal time step for a given accuracy κ, and then we make a small series of simulations (requiring among others less computing power).

The size of the lattice we use is large, about 4 million horizons, and thus, with the optimal time step, the observables are computed very precisely. The point of time when the graphs stop being smooth (have discontinuities) is interpreted as the point where the accuracy is lost. From then onwards, the predictions for the observables can be treated only qualitatively. After careful analysis, we have fixed κ to be 10^{-4} which gives us the time step in the range 0.005 and 0.02.

APPENDIX C: SIZE OF THE LATTICE

Representing the field on a large lattice requires a lot of memory. A single simulation in 2D on a lattice of $2048 \times$

TABLE VI.   Resolution versus lattice size in 2D (upper panel) and in 3D simulations.

n_x	786	1024	1536	2048	3072	4096
δ	10^{-3}	2×10^{-4}	10^{-4}	5×10^{-5}	1×10^{-5}	2×10^{-6}

n_x	80	100	128	160	200	256
δ	7×10^{-5}	4×10^{-5}	10^{-5}	5×10^{-5}	2.5×10^{-6}	6.2×10^{-7}

2048 with $\kappa = 10^{-4}$ requires more than 10 hours of computing time to reach $\eta_{\text{stop}} \sim 100$.

The resolution δ (precision) that we previously discussed is the smallest visible relative change of the field statistics—we estimated this by looking at the plots of surface energy of the walls comparing them to the simulation performed on the largest possible lattice. The results are given in Table VI, for 2D and 3D.

We have found that the logarithm of the resolution δ is linear in the lattice size, and the best fit for 2D is given by

$$\log_{10}\delta = -3.237 - 1.88 \times 10^3 \times n_x^{3/2},$$

$$\delta \sim 10^{-3.237} \times 10^{-(n_x^{3/2}/1526)}.$$

For 3D the logarithm of the resolution is proportional to the power of n:

$$\log_{10}\delta = -3 - 6.55 \times 10^{-4} \times n_x,$$

$$\delta \sim 10^{-3} \times 10^{-(n_x/1526)}.$$

In our simulation, we need these formulas to judge when the number of domain walls is too small to trust the numerical results. Technically, because we are using periodic boundary conditions, after a finite time (which is of the order of the lattice size over the velocity of the wall), a wall that leaves the horizon could return, since it comes to the lattice from the other side. This sets the limit of the simulations. Thus, looking at the simulations, we can see that the average velocity of the walls is 0.5, which means that the return time is approximately twice the lattice size. Thus, this is the absolute upper limit on the useful range of η's.

We have verified that for the lattices we have used, the role of the periodic boundary conditions is negligible.

APPENDIX D: MONITORING OF THE POSITION OF THE MINIMA OF DIFFERENT POTENTIALS

The position of the extrema of the potential is monitored both analytically and numerically.

1. Double-well potential

For the potential

$$V(\phi) \rightarrow V(\phi) - \epsilon V_0 \phi$$

with

$$V(\phi) = V_0\left(\left(\frac{\phi}{\phi_0}\right)^2 - 1\right)^2,$$

the Taylor expansion of the potential is

$$V(\phi) = V_0 + \frac{1}{2}\left(\frac{V_0}{v^2}\right)\phi^2 + \frac{1}{4!}\left(\frac{V_0}{v^4}\right)\phi^4 + \cdots.$$

For a small nondegeneracy parameter ϵ we can easily find the position for the extrema of the potential (maximum)

$$\phi = -\frac{1}{4\phi_0^2}\epsilon - \frac{1}{64\phi_0^8}\epsilon^3 - \frac{3}{1024\phi_0^{14}}\epsilon^5 - \frac{3}{4096\phi_0^{20}}\epsilon^7 \cdots$$

(minimum)

$$\phi = -\phi_0 + \frac{1}{8\phi_0^2}\epsilon - \frac{1}{128\phi_0^5}\epsilon^2 + \frac{1}{128\phi_0^8}\epsilon^3$$
$$- \frac{105}{32\,768\phi_0^{11}}\epsilon^4 + \frac{3}{2048\phi_0^{14}}\epsilon^5 - \frac{3003}{4\,194\,304\phi_0^{17}}\epsilon^6$$
$$+ \frac{3}{8192\phi_0^{20}}\epsilon^7 \ldots,$$

$$\phi = \phi_0 + \frac{1}{8\phi_0^2}\epsilon + \frac{1}{128\phi_0^5}\epsilon^2 + \frac{1}{128\phi_0^8}\epsilon^3$$
$$+ \frac{105}{32\,768\phi_0^{11}}\epsilon^4 + \frac{3}{2048\phi_0^{14}}\epsilon^5 + \frac{3003}{4\,194\,304\phi_0^{17}}\epsilon^6$$
$$+ \frac{3}{8192\phi_0^{20}}\epsilon^7 \ldots.$$

The important thing is the position of the maximum, which we use as the border between the left and right vacuums. One can always find numerically the position of the extrema, via the Newton-Raphson method: $x_{i+1} = x_i - \frac{f(x_i)}{f'(x_i)}$.

2. Runaway potential

For

$$V(s) = \frac{1}{2s}(A(2s + N_1)e^{-(s/N_1)} - B(2s + N_2)e^{-(s/N_2)})^2$$

(where s is canonically normalized), we find the extrema as follows:

$$\frac{dV}{ds} = -\frac{1}{2N_1N_2s^2}e^{-2(s(N_1+N_2)/N_1N_2)}[A(2s + N_1)e^{s/N_2}$$
$$- B(2s + N_2)e^{s/N_1}][AN_2(N_1^2 + 4s^2)e^{s/N_2}$$
$$- BN_1(N_2^2 + 4s^2)e^{s/N_1}].$$

Here, we have two brackets and either the first or the second vanishes. This gives the following conditions:

$$e^{s(N_1 - N_2/N_1N_2)} = \frac{B(N_2 + 2s)}{A(N_1 + 2s)},$$

$$e^{s(N_1 - N_2/N_1N_2)} = \frac{BN_1(N_2^2 + 4s^2)}{AN_2(N_1^2 + 4s^2)}.$$

These two conditions are nonlinear and cannot be solved algebraically, but can be solved iteratively, step by step:

$$s_{(i+1)} = \frac{N_1N_2}{N_1 - N_2}\ln\left[\frac{B(N_2 + 2s_{(i)})}{A(N_1 + 2s_{(i)})}\right],$$

$$s_{(i+1)} = \frac{N_1N_2}{N_1 - N_2}\ln\left[\frac{BN_1(N_2^2 + 4s_{(i)}^2)}{AN_2(N_1^2 + 4s_{(i)}^2)}\right],$$

$$s_{(0)} = \frac{N_1N_2}{N_1 - N_2}.$$

To remove the degeneracy of the vacua, we add a term that looks like $\sim \frac{\epsilon}{s^2}$.

[1] C. L. Bennet *et al.*, Astrophys. J. Suppl. Ser. **148**, 1 (2003); D. N. Spergel *et al.*, Astrophys. J. Suppl. Ser. **148**, 175 (2003); H. V. Peiris *et al.*, Astrophys. J. Suppl. Ser. **148**, 213 (2003).

[2] A. G. Riess *et al.*, Astron. J. **116**, 1009 (1998); Astrophys. J. **607**, 665 (2004); J. L. Tonry *et al.*, Astrophys. J. **594**, 1 (2003).

[3] For a review of topological defects, see A. Vilenkin, Phys. Rep. **121**, 263 (1985).

[4] See, for instance, P. Sikivie, Phys. Rev. Lett. **48**, 1156 (1982); J. Ipser and P. Sikivie, Phys. Rev. D **30**, 712 (1984); I. Wasserman, Phys. Rev. Lett. **57**, 2234 (1986); C. T. Hill, D. N. Schramm, and J. N. Fry, Comments Nucl. Part. Phys. **19**, 25 (1989); L. Kawano, Phys. Rev. D **41**, 1013 (1990); A. Massarotti, Phys. Rev. D **43**, 346 (1991); M. S. Turner, R. Watkins, and L. M. Widrow, Astrophys. J. **367**, L43 (1991).

[5] M. Dine, Phys. Lett. B **482**, 213 (2000).

[6] R. Brustein and P. J. Steinhardt, Phys. Lett. B **302**, 196 (1993).

[7] W. Buchmüller, K. Hamaguchi, O. Lebedev, and M. Ratz, Nucl. Phys. **B699**, 292 (2004).

[8] W. Press, B. Ryden, and D. Spergel, Astrophys. J. **347**, 590 (1989).

[9] S. E. Larsson, S. Sarkar, and P. L. White, Phys. Rev. D **55**, 5129 (1997); H. Casini and S. Sarkar, Phys. Rev. D **65**, 025002 (2001).

[10] D. Coulson, Z. Lalak, and B. A. Ovrut, Phys. Rev. D **53**, 4237 (1996).

[11] L. Conversi, A. Melchiorri, L. Mersini-Houghton, and J. Silk, Astropart. Phys. **21**, 443 (2004).

[12] S. Lola and G. G. Ross, Nucl. Phys. **B406**, 452 (1993).

[13] Z. Lalak, S. Lola, B. Ovrut, and G. G. Ross, Nucl. Phys. **B434**, 675 (1995).

[14] S. Lola, Phys. Lett. B **398**, 23 (1997).

[15] T. Matsuda, Phys. Lett. B **486**, 300 (2000).

[16] T. Garagounis and M. Hindmarsh, Phys. Rev. D **68**, 103506 (2003).

[17] P. P. Avelino, J. C. R. Oliveira, and C. J. A. Martins, Phys. Rev. D **72**, 083506 (2005); **71**, 083509 (2005); Phys. Lett. B **610**, 1 (2005); P. P. Avelino, C. J. A. Martins, and L. Sousa, Phys. Rev. D **78**, 043521 (2008); P. P. Avelino *et al.*, arXiv:0807.4442.

[18] M. Eto, T. Fujimori, T. Nagashima, and M. Nitta, Phys. Rev. D **75**, 045010 (2007); M. Eto *et al.*, Phys. Rev. D **76**, 125025 (2007).

[19] Z. Lalak, B. A. Ovrut, and S. Thomas, Phys. Rev. D **51**, 5456 (1995).

[20] C. Hill and G. Ross, Nucl. Phys. **B311**, 253 (1988); Phys. Lett. B **203**, 125 (1988); A. Gupta, C. Hill, R. Holman, and E. Kolb, Phys. Rev. D **45**, 441 (1992).

[21] S. Coleman, Phys. Rev. D **15**, 2929 (1977).